Forest Ecology and Management 497 (2021) 119494

Contents lists available at ScienceDirect

Forest Ecology and Management

journal homepage: www.elsevier.com/locate/foreco

Investigating linkages between the size-growth relationship and drought, nitrogen deposition, and structural complexity in western U.S. Forests

Christopher E. Looney [a,*], Anthony W. D'Amato [b], Sarah Jovan [c]

[a] USDA Forest Service, Pacific Southwest Research Station, 1731 Research Park Dr., Davis, CA 95618, USA
[b] University of Vermont, Rubenstein School of Environment and Natural Resources, Burlington, VT 05095, USA
[c] USDA Forest Service, Pacific Northwest Research Station, 620 SW Main, Suite 502, Portland, OR 97205, USA

ARTICLE INFO

Keywords:
Growth dominance
Climate change
Air pollution
Competition symmetry
Structural heterogeneity
Lichen bioindicator

ABSTRACT

Understanding how stand structure responds to stresses such as drought and pollution could aid forest managers in evaluating silvicultural treatment success, predicting treatment durability, and designing adaptive management approaches. The size-growth relationship (SGR), a measure of growth partitioning among different size trees in a stand, may provide a means of linking stresses impacting individual trees to forest stand development and growth. No study to date has tested SGR's response to drought and pollution, specifically N deposition, across landscapes. We combined Forest Inventory and Analysis (FIA) stand development and plot-level lichen bioindicator data on N deposition with climate data denoting moisture availability. Using linear regression, we examined SGR, stand structural complexity, individual tree growth and mortality in largely multi-aged, mixed species stands in California, Oregon, and Washington, USA, coniferous and pine-oak forests. Our goals were to determine a) the influence of moisture availability and/or N deposition on SGR, b) whether SGR translates to differences in stand structural complexity over time, and c) the extent to which SGR mediates the impacts of abiotic stress on tree growth and mortality. Consistent with previous research, our results indicated that SGR increased with stand density, indicative of larger trees possessing a disproportionate advantage in aboveground competition for light. SGR declined linearly with stand age, trending over time towards disproportionately slow large-tree growth. SGR strongly increased with low-moderate bioindicated N deposition, which is consistent with past findings that SGR increases with site quality and suggests that N deposition disproportionately increases growth in larger trees. We did not find evidence that drought stress (as indicated by the Palmer Drought Severity Index) influenced SGR. Stands that were already more structurally complex showed further gains in complexity under high SGR (disproportionately rapid large-tree growth), whereas stands that were initially structurally simpler increased in complexity under low SGR (disproportionately slow large tree growth). As such, individual-tree growth and mortality may drive changes in complexity. Our results support the utility of SGR as a predictor of how stress impacts stand structure, but only when accounting for initial structural complexity. Our findings also have implications for the design and durability of silvicultural treatments, given that silvicultural prescriptions often involve the manipulation of tree size distributions. Moreover, these findings underscore the importance of accounting for the historical influence of N deposition on stand development during treatment planning, as well as the likelihood of socioeconomic changes altering N deposition in the future.

1. Introduction

Silviculture seeks to develop effective approaches for sustaining ecosystem services (Puettmann et al., 2009) and lowering vulnerability to global change (Nagel et al., 2017). Within the realm of silviculture, ecological forestry approaches such as variable retention harvesting and irregular shelterwoods can enhance present ecosystem services by increasing structural heterogeneity (Franklin et al., 2007; Raymond et al., 2009). Increased structural heterogeneity may also reduce risks from global change-related stresses such as drought, invasive species, and air pollution, while fostering transitions to future-adapted tree species (Muller et al., 2019). Understanding how stand structure develops in response to stress could allow managers to better evaluate treatment success, predict treatment durability, and guide adaptive

* Corresponding author.
E-mail addresses: christopher.looney@usda.gov (C.E. Looney), awdamato@uvm.edu (A.W. D'Amato), sarah.jovan@usda.gov (S. Jovan).

https://doi.org/10.1016/j.foreco.2021.119494
Received 17 May 2021; Received in revised form 26 June 2021; Accepted 28 June 2021
Available online 16 July 2021
0378-1127/© 2021 Published by Elsevier B.V.

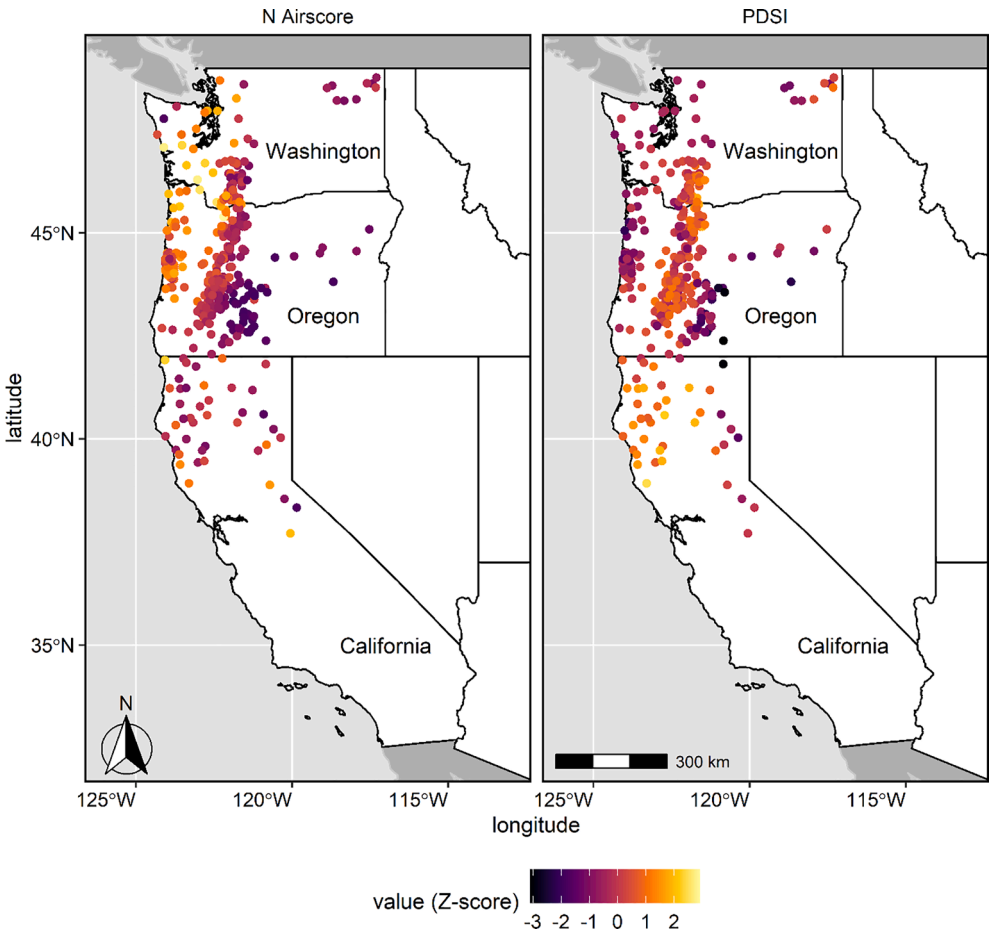

Fig. 1. Map of study plot locations in the U. S. States of California, Washington, and Oregon. Plot locations are based on publicly available (~800 m fuzzed) plot coordinates. The left panel depicts the nitrogen deposition air score (N airscore) within each FIA plot. The right panel summarizes the Palmer Drought Severity Index (PDSI) at each sample plot location based on climate records corresponding with individual-plot remeasurement periods. Values of both indices are converted for Z-scores for consistent display.

management.

Stand response to stress is most often evaluated in terms of growth (Bottero et al., 2017; Jucker et al., 2016) and tree mortality (Zhang et al., 2013). Evidence from long-term stocking studies suggests thinning even-aged stands enhances resistance and resilience of growth to drought (Bottero et al., 2017; Zhang et al., 2019). However, tree sensitivity to stress commonly changes with tree size, leading to within-stand variation in stress effects (Trouillier et al., 2019). Over time, such nuanced stress effects may alter structural complexity (Pretzsch and Dieler, 2010), which may be a more consequential response than stand growth for objectives such as maintaining wildlife habitat or fire risk reduction (Bauhus et al., 2009; Ziegler et al., 2017). Quantifying within-stand variation in growth can aid the design of more efficient silvicultural treatments (Bradford et al., 2010).

The size-growth relationship (SGR) may provide an effective means of linking stresses impacting individual trees to stand development and growth (Forrester, 2019). SGR is a measure of growth partitioning among different size trees in a stand (Pothier, 2017; Pretzsch and Biber, 2010). High SGR indicates disproportionately rapid large-tree growth, which is predicted to reduce variation in tree size during stand development (Forrester, 2019). In contrast, low SGR indicates high small-tree vigor and potential for release from disturbance (Bradford et al., 2010). The size-growth relationship has strong parallels to the concept of competition symmetry (Pretzsch and Dieler, 2010). High SGR values signify partial size asymmetry (larger trees monopolize resources, as with competition for light); a 1:1 correspondence between growth and size signifies perfect size symmetry (resource distribution proportional to tree size), and low values signify partial size symmetry (suppressed growth of large relative to small trees assumed to result from limitations in below-ground water and nutrient resources; Pretzsch and Dieler, 2010; van Kuijk et al., 2008). Although SGR has inconsistent direct effects on stand growth (Dye et al., 2019), it may nevertheless impact stand structure. Over time, high SGR may diversify tree diameter distributions as larger trees accelerate in growth (Forrester, 2019), provided that smaller trees do not experience self-thinning mortality (Pretzsch and Dieler, 2010).

In addition to quantifying trends in stand structural development, increasing evidence suggests SGR is sensitive to environmental fluctuations (Pretzsch and Dieler, 2010). SGR can vary with site quality and in response to stresses such as drought and pollution. Higher SGR is associated with higher site index, an indicator of long-term site productivity (Pretzsch and Dieler, 2010). Temporary declines in SGR are associated with drought in both hardwood and conifer stands (Castagneri et al., 2012; Looney et al., 2016; Pretzsch and Dieler, 2010). A fumigation experiment found tropospheric ozone reduces SGR by disproportionately reducing large tree growth, particularly in wetter years (Pretzsch and Dieler, 2010). Nitrogen (N) deposition may also potentially alter SGR, although its effects remain unclear. In general, N deposition increases tree leaf area and susceptibility to physical damage, drought, and mortality (Carter et al., 2017; Fenn et al., 2020). However, Ibáñez et al. (2018) found that N deposition helped sustain the growth of individual sugar maple *(Acer saccharum* L.) trees under drought, rather than antagonizing water limitation. No study to date has tested how SGR responds to drought and pollution, in particular N deposition, across landscapes.

Pollutants such as N deposition are quite variable over short distances and may be attenuated or concentrated by local topography and stand structure (Jovan et al., 2021). To avoid the resolution limitations and interpolation issues of gridded datasets for N (Walker et al., 2019), land managers in the western U.S. and elsewhere commonly use

Table 1
Description of predictor and response variables used in modeling.

Analysis	Variable	Level	Description	Data source
SGR, ΔSCI, G, M	SGR	Plot	Metsaranta & Lieffer's (2010) index, proportional size vs. growth	FIADB-derived
ΔSCI	ΔSCI	Plot	Periodic change in structural complexity index	FIADB-derived
ΔSCI	SCI	Plot	Initial value of structural complexity index	
SGR, SCI	Stand age	Plot	Estimated predominant breast height tree age	FIADB
SGR, SCI	SDI	Plot	Stand density index*	FIADB-derived
SGR, G	Heat load	Plot	Heat load based on aspect, slope, latitude	FIADB-derived
SGR	N airscore	Plot	N deposition index within FIA plots	Bioindicators DB
SGR	CMD	Plot	Ratio of total precipitation/ actual evapotranspiration	Terraclim
M	REMPER	Plot	Plot remeasurement period (yr)	FIADB
G, M	SDIL	subplot	SDI of trees larger than each subject tree sharing a sample plot	FIADB-derived
G	Growth	Tree	Net sound cubic volume increment (m^3 $tree^{-1}$ $year^{-1}$)	FIADB
M	Status	Tree	Tree status (0 = live, 1 = dead) upon plot remeasurement	FIADB
G, M	DBH	Tree	Initial tree diameter at breast height	FIADB
M	LCR	Tree	Initial tree live crown ratio	FIADB

Note: Abbreviations note explained in the table are as follows: G = individual-tree growth, M = individual-tree mortality, FIADB = Forest Inventory and Analysis Database, Biodindicators DB = FIA lichen macrodatabase, Terraclim = TerraClimate dataset (Abatzoglou et al., 2018). Level indicates whether a variable is assessed plot-wide, within subplots (nested subplots and macroplots), or for individual-trees.

* SDI calculated using the summation method based on individual-tree diameters (Long and Daniel, 1990).

epiphytic lichen communities as inexpensive in-situ bioindicators of long-term N deposition (e.g., Jovan et al., 2021; Root et al., 2015). Lichens derive the majority of essential nutrients such as N directly from the atmosphere (Root et al., 2015), removing the mediating effects of factors such as soils. Lichen species show distinct tolerances for environmental N, with strong correlations between functional group richness/evenness and N deposition (Jovan, 2008). Forest Inventory and Analysis (FIA) lichen bioindicator data has been applied to a broad variety of ecological research (e.g., Jovan et al., 2020, Appendix 1), contributing to a global assessment of N deposition effects on plant diversity (Bobbink et al., 2010) and an investigation into the cascade effects of N eutrophication on ecosystem services in US ecoregions ranging from temperate forest to desert (Clark et al., 2017). However, to our knowledge, no previous study has used lichen bioindicator data to examine N deposition effects on forest stand dynamics.

To investigate how SGR responds to drought and air pollution, we combined FIA stand development and plot-level lichen bioindicator data on N deposition with climate data denoting moisture availability. We examined SGR, stand structural complexity (defined as a gradient ranging from simple, unimodal diameter distributions associated with even-aged stands to right-skewed or multimodal distributions associated with uneven-aged stands; Ducey, 2009), individual tree growth and mortality in largely multi-aged stands in coniferous and pine-oak forests in the U.S. Pacific Coast states of California, Oregon, and Washington. Our goals were to determine a) the influence of moisture availability and N deposition on SGR, including possible interactions between these stressors, b) whether SGR translates to difference in stand structural complexity over time, and c) the extent to which SGR mediates the impacts of abiotic stress on tree growth and mortality. Evaluating SGR as a driver of historical stress-growth-stand structure patterns could potentially aid the management of western U.S. forests, where increasing drought and air pollution may have unanticipated consequences for stand development. More broadly, it will help determine the utility of the metric for assessing the success and durability of silvicultural treatments designed to mitigate global change impacts.

2. Materials and methods

2.1. Study system and plot selection

We based this study on national inventory data from the USDA Forest Service Forest Inventory and Analysis (FIA) program. We selected data from the Pacific Northwest region of FIA, encompassing the states of California, Oregon, and Washington. This region shares a common FIA sampling protocol (Waddel, 2013). The climate is Mediterranean from the coast through the western Sierra and Cascade ranges. Summers are warm and most precipitation occurs in winter as rainfall that becomes snow in the north and at higher elevations. East of the mountain ranges, climate is more arid and continental, with more precipitation occurring as winter snowfall (Western Regional Climate Center, 2021). Incorporating data from across this large region both enhanced sample sizes and assured greater variation in drought and air pollution across time and space. Among the plots selected for this study, elevation ranged from 30 to 2160 m. Publicly available plot coordinates, fuzzed by ~ 800 m from true locations (Bechtold and Patterson, 2005), ranged from 37.53 to 48.77° degrees latitude and from −117.3 to −124.3° longitude (Fig. 1). Mean plot precipitation over the prior 10 years ranged from 240.1 to 5041.0 mm yr^{-1}, and mean annual temperature over the study period from 3.3 to 15.0 °C (PRISM Climate Group, 2019).

We queried forested plots (≥10% canopy cover) falling within a single stand, or "condition" in the FIA database (condition table: condprop_unadj > 0; Woudenberg et al., 2010). We selected plots free of recent treatment or natural disturbance (≥25% of trees per species impacted ; Woudenberg et al., 2010). Under the present annual inventory plot design, 4 × 0.016 ha subplots are used to measure trees (>12.7 cm diameter at breast height (DBH)) and 4 × 0.0013 ha microplots to measure saplings (>2.54 DBH < 12.7 cm). Large trees (generally ≥ 60.1 cm but up to ≥ 76.2 cm DBH depending on locale) are measured on annular macroplots (0.101 ha). Plots are targeted for remeasurement every 10 years, and we included only plots with 8 yr < remeasurement period < 12 yr for consistent growth estimates. At the time of querying (8/14/2020), sampling dates of selected plots ranged from first measurements in 2006 to second measurements in 2018.

We dropped plots that did not have at least 1 lichen bioindicator visit, consisting of a timed survey of up to 2 h by a specially-trained field crew who noted the abundance of all epiphytic macrolichen species using broad abundance classes (Jovan et al., 2020). We also excluded plots with < 10 trees for accurate regression-based SGR estimates and with stand ages < 20 and > 250 years to avoid the confounding influence of succession in the lichen bioindicator community. Lastly, we dropped individual trees with a non-positive net volume increment, assuming these represented cases where growth was within measurement error or reflected cull due to damage, as well as trees on low-productivity plots where preliminary analysis found no net growth. Based on these criteria, from our initial sample of 5,847 plots, we retained 463 plots consisting of a variety of forest types ranging from coastal redwood and Douglas-fir to lower-productivity interior ponderosa pine and foothill oak woodlands (See Appendix Table A.1). Plot densities were higher in Oregon and Washington, reflecting both the higher intensity of bioindicator program sampling on National Forest lands in these states (Jovan et al., 2020) and extensive disturbance in California's southern Sierra Nevada and Transverse Ranges (Preisler et al., 2017).

Table 2
List of different hypothesis models evaluated for size-growth relationship (SGR), structural complexity index (SCI), growth, and mortality responses in this study. Null model terms (e.g., stand age and SDI for SGR) are included in all models for a given response.

Response	Hypothesis	Response varies as a function of:
SGR	SGR0	Null model (stand age, SDI, CMD)
SGR	SGR1	Null model, PDSI
SGR	SGR2	Null model, N Airscore
SGR	SGR3	Null model, PDSI, N Airscore
SGR	SGR4	Null model, PDSI, N Airscore, PDSI × N Airscore
ΔSCI	ΔSCI0	Null model (stand age, SDI, initial SCI)
ΔSCI	ΔSCI1	Null model, SGR
ΔSCI	ΔSCI2	Null model, SGR, SGR × stand age
ΔSCI	ΔSCI3	Null model, SGR, SGR × SCI
G/M	G0/M0	Null model (DBH, heat load, SDIL, CMD, plus rem.per for mortality models)
G/M	G1/M1	Null model, SGR
G/M	G2/M2	Null model, SGR, DBH × SGR
G/M	G3/M3	Null model, PDSI
G/M	G4/M4	Null model, N airscore
G/M	G5/M5	Null model, N airscore, PDSI
G/M	G6/M6	Null model, SGR, PDSI
G/M	G7/M7	Null model, SGR, N airscore
G/M	G8/M8	Null model, SGR, N airscore, PDSI
G/M	G9/M9	Null model, DBH × SGR, PDSI
G/M	G10/M10	Null model, DBH × SGR, N airscore
G/M	G11/M11	Null model, SGR, N airscore, PDSI, N airscore × PDSI

Note: Please see Table 1 for abbreviations of model responses and terms.

2.2. Size-growth relationship

We selected Metsaranta and Lieffer's (2010) index to represent SGR in this study based on its relative ease of calculation and use of standardized tree growth and size, which facilitates interpretation (Forrester, 2019). Metsaranta and Lieffer's (2010) SGR is based on the slope of the linear regression between individual-tree proportional growth and proportional initial volume. Both growth and volume are center log-ratio transformed (Aitchison, 1986), making individual tree contributions proportional to stand totals. These transformations linearize relationships between growth and volume, an assumption we visually confirmed for a random sample of trees (N = 50). We dropped plots with < 10 trees to assure adequate sample sizes for linear regression (Ellison and Gotelli, 2004). We calculated a single plot estimate of SGR based on plot trees pooled across subplots. We based SGR on net sound cubic volume and volume increment, which discounts volume and growth lost to rot, cull, or stem breakage (Table 1; Woudenberg et al., 2010). Dead trees and ingrowth were excluded from SGR calculations. The average number of trees included in SGR estimates was 27.0 (SD = 12.3).

Values of SGR = 1 signify tree growth directly proportional to size, or perfect size-symmetry (Metsaranta and Lieffers, 2010; Pretzsch and Dieler, 2010). Values > 1 signify disproportionately high large-tree growth, corresponding with partial size-asymmetric competition. Values < 1 signify disproportionately low large tree growth, or partial size-symmetry. Values ~ 0 signify equal (absolute) growth among trees regardless of size.

2.3. Climate and N deposition

We summarized within-site drought stress using the Palmer Drought Severity Index (PDSI; Palmer, 1965). We represented long-term across-site variation in moisture stress using the climatic moisture deficit (CMD), defined as the difference between potential evapotranspiration (PET) and actual evapotranspiration (AET). Following Stephenson (1998), potential evapotranspiration is defined as evapotranspiration from a standard crop given the availability of sufficient water, while actual evapotranspiration is the evaporative water loss from a given site covered by a hypothetical standard crop given observed water availability. This index has strong performance in predicting tree species distributions (Lutz et al., 2010) and growth across landscapes (Restaino et al., 2016). In contrast, precipitation and temperature variables may yield misleading inferences regarding growth-climate relationships based on periodic growth data and space-for-time substitution (Klesse et al., 2020). We used 4 km gridded PDSI estimates from Terraclim, which are based on a Thornthwaite-Mather model (Abatzoglou et al., 2018). We joined PDSI estimates to sample plot locations with bilinear interpolation using the raster package (Hijmans et al., 2020) for R (R Core Team, 2018). Monthly PDSI records were summarized to mean periodic PDSI based on the most recent date and interval between measurements for each plot. For CMD, we used long-term (1961–1991) 4 km-resolution norms from the UBC Climate NA project (Wang et al., 2016) incorporated into the FIA lichen bioindicators database for each true FIA plot location (Jovan et al., 2020).

'N airscores' is the primary species composition index used to estimate N with the FIA lichen dataset (Geiser et al., 2019). In brief, N airscores are the average deposition tolerance of all lichen species occurring at a site. Low scores mean the site has a high proportion of deposition-sensitive species tolerating only "clean" conditions; high scores mean the site has a high proportion of deposition-tolerant species characteristic of "dirty" conditions. As N airscores are weighted by the abundance of species found during the FIA lichen bioindicator visit, each species has more emphasis on parts of the deposition gradient where it is more abundant and less emphasis where it is rare. The distribution of sample plots also reflected more intense bioindicator sampling in the Pacific Northwest states of Washington and Oregon (Fig. 1). The comparatively fewer plots in California were restricted to the northern half of the state. The calculations used to synthesize the N airscore index from lichen community data help minimize age-related effects and, thus, the confounding influence of succession on N airscore estimates (Geiser et al. 2019). Additionally, the age range of trees included in this study (≥20 ≤ 250 years) eliminated the extremes of successional stages, i.e., stands too young to be colonized by lichen and stands dominated by a special community of rare old-growth lichens.

Periodic mean plot PDSI ranged from −1.64 (mild drought) to 0.94 (mildly moist), averaging −0.18 (SD = 0.41). Periodic PDSI values were lower east of the Sierra Nevada and Cascade Range in California and Oregon, as well as along the central Oregon coast. Mean annual climatic water deficit ranged from 11.1 mm yr^{-1} (most humid) to 862.0 mm yr^{-1} (most xeric), averaging 358.3 mm yr^{-1} (SD = 169.0). Long-term climatic moisture deficit generally decreased with latitude and proximity to the coast. The average N airscore among plots selected for this study ranged from 1.6 (cleanest) to 9.6 (most polluted), with an average score of 4.7 (SD = 1.7). Plots east of the Cascade Range in eastern Oregon had the cleanest air scores. Areas of notably high N deposition included the California central valley, western Washington, and northwestern Oregon.

2.4. Linear plot-level SGR and structural complexity models

We built a series of competing generalized linear models of SGR as a function of PDSI and the lichen index of N deposition (i.e., N airscores). Stand age, stand density, and climatic moisture deficit terms were included in all models. Stand age has generally been linked to declining SGR following stand establishment (Binkley et al., 2006; Pothier, 2017). Stand density is also important predictor of SGR, influencing the strength of many interactions between neighboring trees, such as light competition, that affect tree resource use efficiency (Pothier, 2017). We used stand density index (SDI; Reineke, 1933), based on the summation of individual-tree SDI to accommodate irregular stand structures (Long and Daniel, 1990). The size-growth relationship is also sensitive to general site quality (Pretzsch and Dieler, 2010). We chose long-term CMD as a basic climatic indicator of site quality, as tree growth-based indicators such as site index incorporate soil nutrient status (Dănescu et al., 2017), potentially obscuring N deposition impacts. Our null hypothesis model was that SGR varied as a function of stand age, SDI, and

long-term CMD. Alternative hypothesis models examined the individual, combined, and interactive influences of recent PDSI and N deposition (Table 2).

Higher values of SGR are divergently predicted to either increase (Forrester, 2019) or decrease (Pretzsch and Dieler, 2010) stand structural diversity. To determine whether SGR influences structural diversity, and by extension, mediates any PDSI or N deposition effects, we modeled the response of Ducey's (2009) SDI-based index of structural complexity to SGR. Because quadratic mean diameter varies depending on distribution skew, Reineke's (1933) SDI commonly underestimates stocking in structurally complex stands where mean tree size is less than the median (Ducey, 2009). The ratio of conventional to summation SDI therefore indicates structural complexity. For ease of interpretation, we rescaled this ratio to form a structural complexity index:

$$SCI = 1 - \left(\frac{SDI_{Reineke}}{SDI_{summation}}\right)$$

Where $SDI_{Reineke}$ is stand density index, calculated using Reineke's QMD method, and $SDI_{summation}$ is the additive SDI of individual trees. Values > 1 indicate multimodal or reverse-J DBH distributions more characteristic of uneven-aged stands (Ducey, 2009). Values ~ 1 are indicative of even-aged stands with normal diameter distributions.

We analyzed the change in SCI between plot measurements (ΔSCI) using generalized linear modeling. Our null ΔSCI model included SCI change as a function of stand age, site class, SDI, and initial SCI (Table 2). Our first alternative model added the main effect of SGR to these terms. A second alternative model examined whether an SGR × initial SCI interaction additionally influenced ΔSCI. The third alternative model investigated whether SGR instead interacted with stand age to affect ΔSCI.

2.5. Linkages among SGR, stand structural complexity, tree growth, and mortality

The size-growth relationship is thought to primarily reflect the growth efficiency of large trees rather than smaller stems (Baret et al., 2017). In addition, a retrospective study of boreal quaking aspen (*Populus tremuloides* Michx.) found that tree mortality may drive variation in SGR, particularly over longer reconstructions (Metsaranta, 2020). To better illuminate the roles of size-dependent growth and mortality on SGR, we examined individual-tree growth records. We also used this analysis to infer whether these processes contributed to any observed SCI-SGR relationships.

Our individual-tree mortality analysis was based on all trees entering the study alive (N = 15,706 trees), whereas growth analyses censored trees that died between measurements to focus on survivor growth only (N = 13,529 trees). For growth, we used annual net sound volume increment as per stand-level models. For mortality, we used binary live/dead tree status at the time of remeasurement. We followed widespread individual-tree modeling approaches to build null models of basic predictors (Crookston and Dixon, 2005). Our null tree growth model included initial tree diameter, heat load (McCune, 2007), and competition based on relative tree sizes. Our competition index (SDIL; del Río et al., 2014) was based on subplot-level SDI but modified as follows to only include subplot neighbors larger than each subject tree:

$$SDIL = \sum_{\substack{j=1 \\ D_j > D_i}}^{n} \left(\frac{D_j}{25}\right)^{1.605}$$

where D_i is the diameter of target tree *i*, D_j is the diameter of plot neighbor tree *j*, and *n* is the total number of subplot neighbors. Our null tree mortality model included the terms of initial tree diameter, and SDIL. In addition, we included live crown ratio (LCR; crown length/total tree height), a common indicator of tree vigor (Zarnoch et al., 2004). To represent long-term site moisture, we included 1961–1991 CMD norms in both sets of models. We also included remeasurement period to account for the 8–12 yr observation window among plots. We used linear mixed modeling for SGR and SCI models with a Gaussian error distribution. To help control for differences in mean SGR and SCI among forest types, we included FIA forest type as a random effect. Individual-tree growth models contained the random effect of plot and subplot nested within plot, as well as a separate random effect of tree species to avoid the confounding influence of species composition. Individual-tree mortality models only included plot and species random effects due to the rarity of mortality within individual subplots.

Based on these null growth and mortality models, we created 11 alternative models for each individual-tree response (Table 2). Our first alternative examined the main effect of SGR on growth and mortality. The second alternative included the main effect of SGR, as well as the SGR × DBH interaction. Alternatives 3–5 examined support for PDSI, N airscore, and combined PDSI and N airscore effects on individual-tree performance. Alternatives 6–8 iteratively compared the individual and combined effects of PDSI and N airscore in addition to SGR. Alternatives 9 and 10 examined the main effects of SGR and the initial diameter × SGR interaction in addition to PDSI and N airscore, respectively. The final alternative included the main effects of PDSI, N airscore, SGR, and the PDSI × N airscore interaction. Support for an interaction between SGR and DBH in models 2, 9, and 10 would provide evidence that SGR altered the size-dependence of growth or mortality. In the case of models 6–11, substantial support for PDSI and N effects in the presence of an SGR term would suggest SGR does not fully mediate these effects.

2.6. Statistical procedures and model selection

We used the information-theoretic framework with corrected Akaike's information criterion (Sugiura, 1978) to compare evidence for alternative hypothesis models (Burnham and Anderson, 2002). We considered models plausible and warranting inference when ΔAICc values were within 6 units of the best-approximating model that did not contain better-supported nested models (Richards, 2008). We also dropped models with higher AICc support if they were within 2 ΔAICc of simpler alternatives (Burnham and Anderson, 2002). To aid readers in evaluating relative model support, we calculated the evidence ratio, which indicates the likelihood of the best-approximating model being valid relative to competing models (Burnham and Anderson 2002).

We confirmed the linearity of bivariate relationships among SGR, ΔSCI, net sound cubic volume growth, and predictor variables. We examined residuals plots to assess model assumptions of normal residuals, linearity, and homogeneous variance. We used log-gamma models for individual-tree growth. We modeled binary tree status (live/dead) data using a logit link to the binomial error distribution. We inspected model residuals for normality of residuals, homoscedasticity and linearity. We log-transformed SDI in plot-level SGR and SCI models, and log-transformed initial diameter in individual-tree growth models to meet these model assumptions. Predictor variables were scaled and centered (converted to Z-scores) for analysis and back-transformed for presentation.

We performed all generalized linear mixed modeling with the glmmTMB package (Magnusson et al., 2018) for R (R Core Team, 2018) using maximum likelihood estimation. We used the MuMIn package (Bartoń, 2017) to perform model comparisons with AICc and calculate conditional (fixed plus random effects) R^2 for mixed gaussian models. We calculated the area under the receiver operating characteristic curve (AUC) for binomial tree mortality models. We used simulated residuals plots to perform mixed model diagnostics (Hartig, 2018). We evaluated variance inflation factors (VIFs) as a diagnostic of multicollinearity. We found that VIFs did not exceed 3 for any model term, indicating low to moderate collinearity (James et al., 2013). See Appendix Table A.2 for a correlation matrix between variables and predictors for each set of models.

Table 3
Plausible plot-level size-growth relationship (SGR) and structural complexity index (SCI) models based on model selection with corrected Akaike's information criterion (AICc).

Response	Hypos	Model terms						logLik	ΔAICc	ER	R^2
		SDI	Stand age	N airscore	CMD	SGR	SGR × SCI				
SGR	SGR3	x	x	x				−12.7	0	1	0.19
	SGR1	x	x					−26.08	24.7	0	0.13
ΔSCI	ΔSCI5	x	x			x	x	1169.4	0	1	0.2
	ΔSCI1	x	x					1160.54	15.64	0	0.14

Note: Please see Table 1 for abbreviations regarding model terms and responses, and Table 2 for descriptions of hypotheses. Other abbreviations are as follows: Hypos = hypothesis, logLik = log-likelihood, ΔAICc = difference in model support (corrected Akaike's information criterion) relative to best-approximating model, ER = evidence ration, R^2 = coefficient of determination.

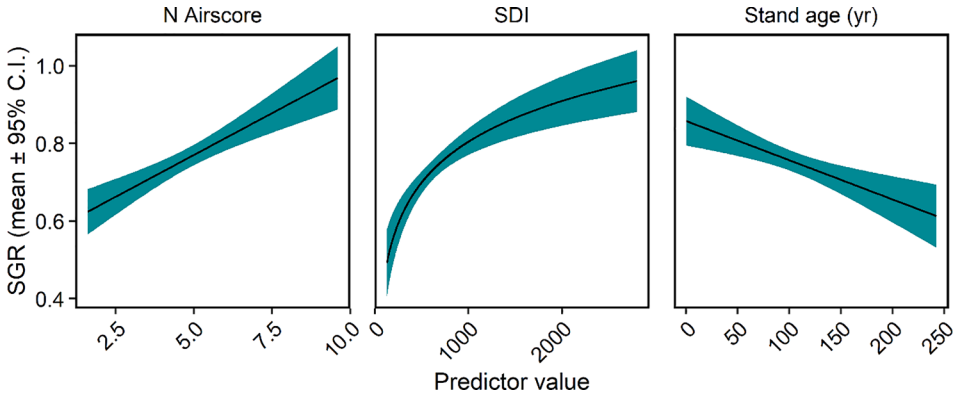

Fig. 2. Predicted values of the size-growth relationship (SGR) as functions of nitrogen deposition air score (N airscore), stand density index (SDI), and stand age (yr). Model predictions represent estimated marginal means (lines) and 95% confidence intervals (shaded bands), calculated while holding other predictors constant at their means.

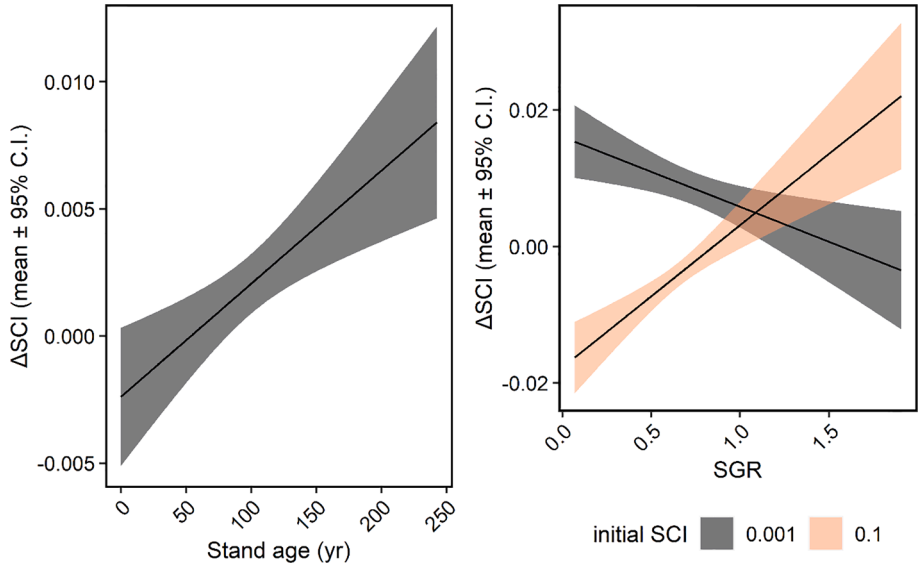

Fig. 3. Predicted values of the structural complexity index (SCI) as functions of stand age (yr) and the size-growth relationship (SGR). Model predictions represent estimated marginal means (lines) and 95% confidence intervals (shaded bands), calculated while holding other predictors constant at their means. For SGR, SDI is back-transformed from the log scale used in analysis.

3. Results

3.1. Plot-level responses: Size-growth relationship and structural complexity

The SGR on sampled plots was generally < 1 (partial size symmetry), ranging from 0.07 to 1.90 and averaging 0.74 (SD = 0.27, see Appendix Table A.3 for complete summaries of response and predictor variables). The best-approximating SGR model described SGR as a function of stand age, SDI, and N deposition (Table 3). We found that SGR declined linearly towards greater size symmetry with stand age (Fig. 2). SGR exhibited a non-linear increase with SDI. Holding other factors constant, mean SGR ranged from partial size symmetry under low SDI to nearly perfect size symmetry at high SDI, increasing less steeply at higher

Table 4
Plausible individual-tree growth and mortality models based on model selection with corrected Akaike's information criterion (AICc).

Response	Hypothesis	Model terms*									logLik	ΔAICc	ER	R^2
		DBH	SDIL	Heat load	LCR	REMPER	SGR	N airscore	CMD	SGR × DBH				
Growth	G3	x	x	x			x	x	x	x	−5078.26	0.00	1.00	0.79
	G1	x	x	x							−5125.70	947.73		0.75
Mortality	M3	x	x		x	x	x			x	−1703.82	0.00	0.98	0.67
	M1	x	x		x	x					−1709.47	7.29	0.01	0.67

Note: Please see Table 1 for descriptions of model responses and terms. Other abbreviations are as follows: logLik = log-likelihood, ΔAICc = difference in model support (corrected Akaike's information criterion) relative to best-approximating model, ER = evidence ration, R^2 = coefficient of determination based on conditional (combined random and fixed) effects.

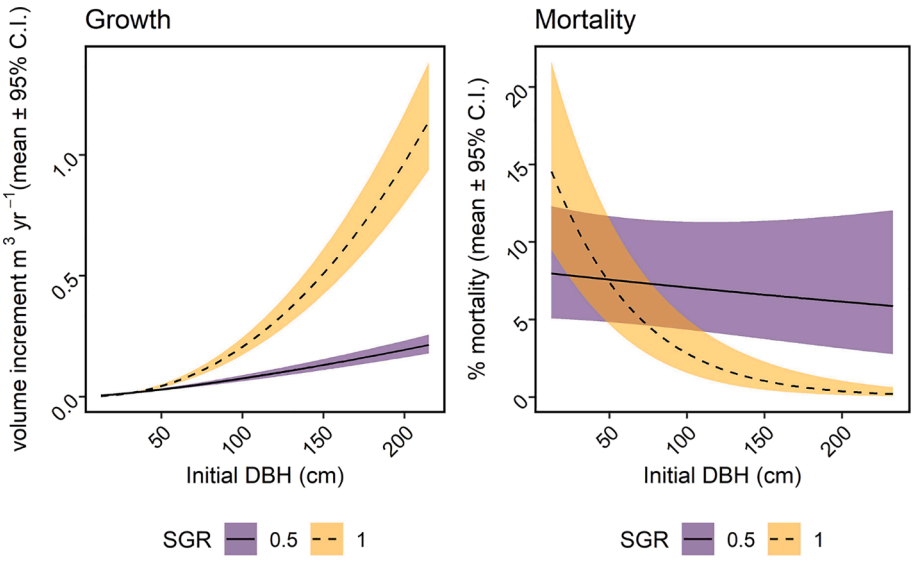

Fig. 4. Interaction plots based on model predictions for the best-supported models of individual-tree growth (left panel) and mortality (right panel). Displayed along the y-axis, growth is defined as net cubic sound volume growth (m^3 yr^{-1}), while mortality reflects the status (0 = living, 1 = dead) of live trees entering the study upon plot remeasurement. The x-axis shows initial tree diameter at breast height (DBH (cm)). The interaction between DBH and the size-growth relationship (SGR) is depicted for low (0.5) and high (1.0) values of SGR based on the range of the data, roughly corresponding with the 1st and 3rd quartiles of SGR. Model predictions are back-transformed from the log scale for growth, and cumulative log–log scale for mortality.

values. The size-growth relationship increased with N airscore, such that SGR was higher (i.e., large trees grew disproportionately faster) on more polluted plots. SGR varied by approximately 40% depending on N airscore, corresponding with a shift from partial size symmetry on low-pollution plots to perfect size asymmetry on the most polluted plots. The size-growth relationship did not vary with long-term CMD. The only models that included PDSI and had substantial AICc support were more complex variants of the best-supported model. The null model (ΔAICc = 6.2) did not have substantial support based on our ΔAICc threshold of 6.

SCI ranged from nearly 0 (0.008) to near the theoretical maximum of 0.198 (Ducey, 2009) and averaged 0.061 (SD = 0.036). Mean ΔSCI between plot measurements was 0.001 (SD = 0.014) and ranged from −0.138 to 0.081. We found greatest AICc support for the model describing ΔSCI as a function of SDI, stand age, initial SCI, the main effect of SGR, and the initial SGR × SCI interaction. Under this model, ΔSCI showed a positive, linear increase with stand age and did not vary with SDI (Fig. 3). We found that the response of ΔSCI to SGR was contingent on initial SCI. Under low initial SCI (structurally simple stands), ΔSCI varied little with SGR. In stands with high initial SCI (structurally complex stands), ΔSCI ranged from negative (declining structurally complexity) when SGR was low to positive when SGR was high. Neither the null model, which dropped SGR, nor an alternative model that added an SGR × stand age interaction had substantial AICc support.

3.2. Tree-level responses: Growth and mortality

The best-approximating volume growth model included the null model terms of initial DBH, SDIL, CMD, and heat load, the main effects of N airscore, and SGR, and the DBH × SGR interaction (Table 4). Growth increased with DBH and N airscore, while decreasing with SDI (see Appendix A.1 for a complete graphical summary). Growth was neutral with respect to heat load and CMD. We found that SGR strongly interacted with DBH, such that growth increased strongly with DBH on plots with high SGR (i.e., disproportionately faster growth of large trees; Fig. 4). The growth of trees with an initial DBH of less than approximately 30 cm was higher on plots with low SGR. Above this tree size threshold, growth became increasingly more rapid with increasing diameter on high SGR plots. We found no plausible support for any competing growth models.

Mean annual plot mortality rates were 1.2% (Sheil and May 1996). Tree mortality was best described by the model that included the null model terms (initial DBH, LCR, SDIL, CMD and remeasurement period; Appendix 2), PDSI, SGR, and the SGR × DBH interaction. Mortality risk declined with LCR and PDSI (moister conditions; see Appendix Fig. A.2 for a complete graphical summary). Mortality odds varied little with respect to SDIL and remeasurement period had a negligible effect on mortality (Fig. 4). Under the DBH × SGR interaction, mortality odds steeply declined with increasing DBH under high SGR and remained constant with DBH under low SGR. Small trees were, therefore, at comparatively higher risk of mortality under high SGR, while larger trees were at relatively greater risk at low SGR. A model dropping the N airscore main effect but retaining the SGR × DBH interaction also had substantial support (ΔAICc = 4.26). No other model had substantial AICc support, including the null model.

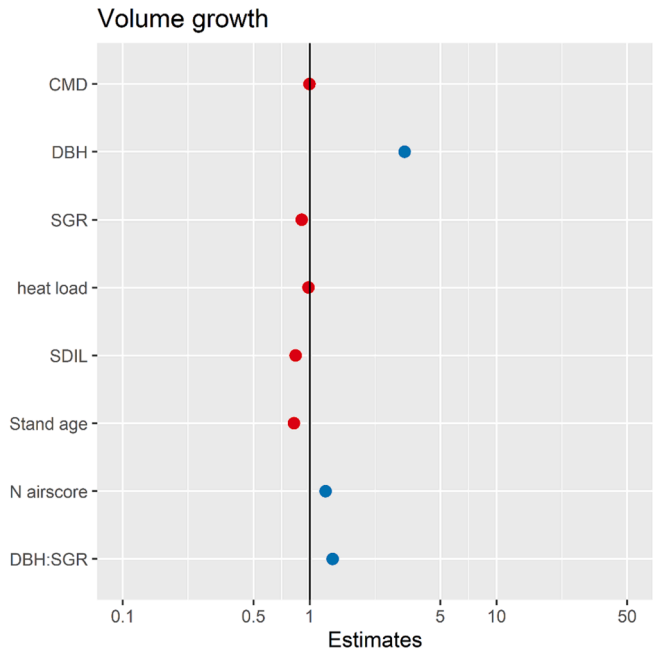

Fig. A.1. Growth model coefficients plot showing the influence of predictors on individual-tree net sound volume increment. Terms (y-axis) correspond to those in the best-approximating growth model and include initial diameter at breast height (DBH), the size-growth relationship (SGR), stand density index of larger neighbors sharing an FIA subplot (SDIL), and the DBH × SGR interaction. The x-axis displays log-scale effects. Dots signify means and error bars 95% confidence intervals; confidence intervals are not visually distinguishable from means due to low variability. Coefficients represent ratios relative to mean growth; a coefficient overlapping with 1 signifies a neutral effect. Coefficients < 1 and > 1 signify negative and positive growth effects, respectively.

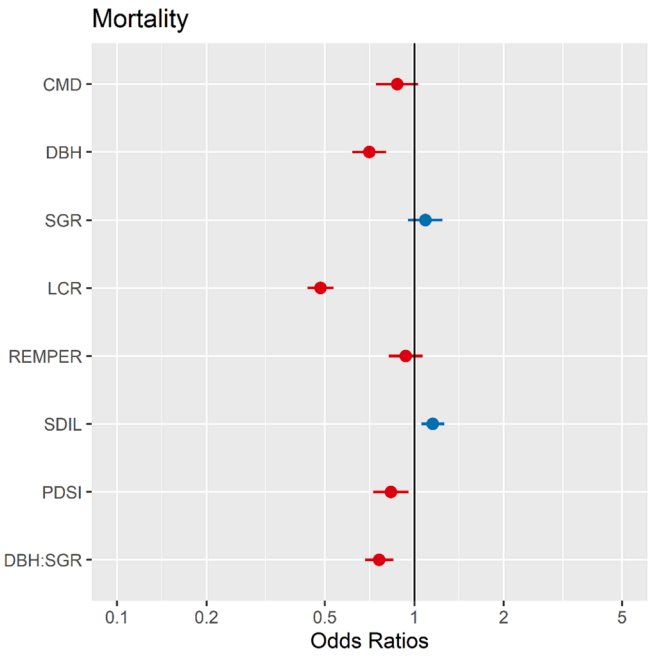

Fig. A.2. Mortality model coefficients plot showing the influence of predictors on individual-tree mortality risk ratios. Terms (y-axis) correspond to those in the best-approximating growth model and include initial diameter at breast height (DBH), the size-growth relationship (SGR), stand density index of larger neighbors sharing an FIA subplot (SDIL), and the DBH × SGR interaction. The x-axis displays log-scale effects. Dots signify means and error bars 95% confidence intervals. Coefficients represent risk ratios relative to mean mortality; a coefficient overlapping with 1 signifies a neutral effect. Coefficients < 1 and > 1 signify decreased and increased mortality risk, respectively.

4. Discussion

4.1. General stand development influences on SGR

Partially size-symmetric SGR (values < 1) was predominant across our study network of conifer-dominated inventory plots. Consistent with previous research, SGR increased with increasing stand density, indicative of greater aboveground competition and a disproportionate advantage of large trees at acquiring light resources (Forrester, 2019). Furthermore, we found that SGR declined linearly with stand age, trending over time consistently towards greater partial size-symmetry (disproportionately low large-tree growth). Binkley et al. (2004) hypothesized that as stands develop, growth shifts from size-asymmetry (large trees disproportionately suppress growth of smaller trees) towards size-symmetry (access to resources is directly proportional to tree size). In support of this hypothesis, we found that SGR consistently declined towards greater size-symmetry with stand age when controlling for stand density and abiotic stress. The decline in SGR with stand age was apparent in both multiple regressions, which adjusted for SDI, and simple bivariate correlations, suggesting the decline in large tree growth efficiency over time was not an artifact of stand age being positively correlated with stand density. Lower SGR in old stands may reflect autogenic processes, such as nutrient limitation, hydraulic limitation, or crown shyness adversely impacting the growth of larger trees (Smith and Long, 2001), or factors such as improved lower canopy microclimates favoring the growth of smaller trees (Forrester, 2019). A positive correlation between SCI and stand age suggest older stands are also more likely to be uneven-aged. Large trees in older, uneven-aged stands may display low SGR as a result of low competition for light. We also noted that mean values even for the youngest stands were indicative of partial size-symmetry (disproportionately slow growth of large trees). Although size-asymmetric SGR appears to be prevalent in certain species (Doi et al., 2010; Metsaranta and Lieffers, 2010), partial size-symmetric growth appears more common among both natural coniferous and hardwood-dominated stands (Dye et al., 2019; Pothier, 2017).

4.2. N deposition, moisture stress, and SGR

We found that SGR strongly increased with bioindicated N deposition, a pattern consistent with findings that SGR increases with site quality (Pretzsch and Dieler, 2010). Compared to ozone damage, which has a neutral-negative influence on the growth of most tree species, low-moderate rates of N deposition commonly have neutral-to-positive effects (Fenn et al., 2020; Horn et al., 2018). The positive influence of N deposition on SGR suggests that N deposition disproportionately increases growth in larger trees. Nutrient limitation has been hypothesized as a key factor behind the age-related growth decline in forests (Gower et al., 1996), a decline which is, in turn, thought to primarily manifest in large tree growth (Binkley, 2004). This decline in large tree growth rates has been theorized to reflect declining tree allocation to leaf area production and photosynthetic efficiency (Baret et al., 2017). N deposition may sustain growth by countering declines in leaf area that typically follow canopy closure early in stand development (Long et al., 2004).

Considering the relatively moderate maximum deposition rates estimated for the plots in this study (<10 kg N ha-1 yr-1; Jovan et al., 2020), relationships between SGR and N deposition could become negative under more intense pollution (Carter et al., 2017). The most intensely polluted plots in southern California were excluded from this study based on our requirements that plots have consistently regular longitudinal data, lack recent major disturbance, and fall within a single stand, possibly preventing our study from capturing any nonlinear SGR-N deposition relationships in chronically N-saturated stands. More

Table A.1
Mean relative density, tree height, and DBH by major species (>1% of relative stand density index).

Species	Species code	Mean % relative SDI	Mean height (m)	Mean diameter (cm)	N carbon increment response*	N response citation
Pseudotsuga menziesii	PSME	31.70	30.6	48.0	neutral	Horn et al. (2018)
Pinus ponderosa	PIPO	14.79	18.7	36.4	neutral	Horn et al. (2018)
Tsuga heterophylla	TSHE	6.08	21.7	31.8	increase	Horn et al. (2018)
Pinus contorta	PICO	5.77	14.8	20.0	increase	Horn et al. (2018)
Abies concolor	ABCO	4.70	20.0	36.7	N/A	N/A
Juniperus occidentalis	JUOC	4.28	8.3	22.4	N/A	N/A
Abies grandis	ABGR	3.69	19.0	29.1	N.S.	Fenn et al. (2020)
Abies amabilis	ABAM	2.96	18.7	29.2	increase	Fenn et al. (2020)
Alnus rubra	ALRU2	2.70	19.5	25.5	unimodal	Horn et al. (2018)
Thuja plicata	THPL	2.64	21.0	38.9	increase	Horn et al. (2018)
Calocedrus decurrens	CADE27	1.91	19.1	42.2	unimodal	Horn et al. (2018)
Quercus Chrysolepis	QUCH2	1.88	9.0	23.0	neutral	Horn et al. (2018)
Tsuga mertensiana	TSME	1.85	16.5	30.0	decrease	Horn et al. (2018)
Pinus jeffreyi	PIJE	1.76	22.1	46.7	neutral	Fenn et al. (2020)
Larix occidentalis	LAOC	1.74	26.4	29.7	N.S.	Fenn et al. (2020)
Quercus kelloggi	QUKE	1.65	13.5	25.0	N.S.	Fenn et al. (2020)
Abies lasiocarpa	ABLA	1.64	13.0	21.4	neutral	Horn et al. (2018)
Lithocarpus densiflorus	LIDE3	1.35	15.6	23.8	increase	Horn et al. (2018)
Arbutus menziesii	ARME	1.32	14.2	25.7	increase	Horn et al. (2018)
Acer macrophylla	ACMA3	1.16	18.6	25.9	N/A	N/A
Pinus lambertiana	PILA	1.14	24.9	46.1	increase	Fenn et al. (2020)
Picea engelmanii	PIEN	1.01	24.2	39.4	increase	Fenn et al. (2020)
Quercus garryana	QUGA4	1.00	8.8	19.2	increase	Horn et al. (2018)
Pinus monticola	PIMO	0.92	19.3	38.2	unimodal	Horn et al. (2018)
Sequoia sempervirens	SESE3	0.90	27.7	49.5	increase	Horn et al. (2018)

Note: SDI = stand density index, N = nitrogen.
* Unimodal carbon increment-N deposition responses are in all cases positive, quadratic relationships. References: Horn et al. (2018); Fenn et al. (2020).

Table A.2
Correlation matrices for variables in tree-level and stand-level analyses, based on Pearson's correlation coefficient.

Variable	Tree-level analyses								
	Stand age	DBH	Growth	SDIL	Heat load	SGR	CMD	N airscore	Status
Stand age	1.00	0.32	0.12	0.15	−0.01	−0.19	−0.05	−0.29	−0.01
DBH	0.32	1.00	0.59	−0.33	0.01	−0.07	−0.08	0.04	−0.04
Growth	0.12	0.59	1.00	−0.23	−0.02	−0.01	−0.07	0.11	−0.03
SDIL	0.15	−0.33	−0.23	1.00	−0.07	0.13	−0.14	0.01	0.00
Heat load	−0.01	0.01	−0.02	−0.07	1.00	−0.15	0.08	−0.11	0.06
SGR	−0.19	−0.07	−0.01	0.13	−0.15	1.00	−0.07	0.28	0.09
CMD	−0.05	−0.08	−0.07	−0.14	0.08	−0.07	1.00	−0.35	0.10
N airscore	−0.29	0.04	0.11	0.01	−0.11	0.28	−0.35	1.00	−0.03
Status	−0.01	−0.04	−0.03	0.00	0.06	0.09	0.10	−0.03	1.00

Variable	Stand-level analyses						
	Stand age	SDI	SGR	CMD	N airscore	ΔSCI	Initial SCI
Stand age	1.00	0.35	−0.18	−0.05	−0.31	0.07	0.38
SDI	0.35	1.00	0.16	−0.28	0.08	0.12	0.13
SGR	−0.18	0.16	1.00	−0.12	0.31	0.17	−0.26
CMD	−0.05	−0.28	−0.12	1.00	−0.39	−0.07	0.10
N airscore	−0.31	0.08	0.31	−0.39	1.00	0.05	−0.15
ΔSCI	0.07	0.12	0.17	−0.07	0.05	1.00	−0.36
Initial SCI	0.38	0.13	−0.26	0.10	−0.15	−0.36	1.00

Notes: *Status (1 = dead, 0 = living) is summarized to the plot level for this table. Abbreviations are as follows: SDI = Stand density index, SGR = size-growth relationship, CMD = climatic moisture deficit, N = Nitrogren, SCI = structural complexity index, SDIL = plot-level SDI comprised of trees larger than a given subject tree, DBH = diameter at breast height.

intense N deposition could lower tree resilience to disturbances such as drought or insect defoliation by reducing root growth and non-structural carbohydrate reserves (Li et al., 2018). Deposition may also adversely affect soil chemistry through the leaching of plant-essential cations and soil acidification (Bowman et al., 2008).

We did not find evidence that drought stress, as indicated by PDSI, influenced SGR. Compared to N deposition, which was assessed directly on the FIA plots, our climate analysis was based on gridded data. Nevertheless, we found evidence for a substantial, negative influence of PDSI on individual-tree mortality, suggesting SGR-PDSI relationships were genuinely weak rather than obscured by limited resolution. Previous studies have found inconsistent SGR-climate relationships. Pretzsch and Dieler (2010) found that SGR in *Picea abies* [L]. (Karst) (Norway spruce) was more symmetric in drought years, whereas *Fagus sylvatica* L. (European beech) SGR did not vary significantly. Other studies of SGR report that climate either had insignificant (Castagneri et al., 2012; Metsaranta and Lieffers, 2010) or inconsistent relationships with SGR among stands of a single species (Looney et al., 2016). Previously, higher SGR has been linked with higher site quality (Pretzsch and Biber, 2010). Site quality, in turn, integrates soil nutrition, soil physical characteristics, physiographic setting, and climatic factors (Dănescu et al., 2017). Considering the lack of SGR responses to either long-term CMD or periodic PDSI, soil nutrition appears to more consequential than moisture stress in regulating SGR in our study systems.

Table A.3
Summary of response and predictor variables.

Variable	Mean	SD	Median	Min	Max	Range	S.E.
SCI	0.06	0.03	0.06	0.01	0.20	0.19	0.00
ΔSCI	0.00	0.01	0.00	−0.14	0.08	0.22	0.00
Stand age	97.80	53.04	90.00	0.00	242.50	242.50	2.72
SDI*	740.68	403.85	682.31	128.36	2801.65	2673.29	20.69
SGR	0.74	0.28	0.73	0.07	1.90	1.83	0.01
CMD	25.39	13.89	21.09	6.45	65.15	58.70	0.71
Net sound volume m^3	2287.83	2912.53	1142.68	29.00	17563.36	17534.37	149.21
Net annual sound volume increment (m^3 yr^{-1})	40.34	42.82	28.59	2.43	526.63	524.21	2.19
Remeasurement Period (yr)	9.98	0.33	10.00	8.70	11.60	2.90	0.02
Aspect	180.94	103.11	180.00	0.00	360.00	360.00	5.58
Elevation (m)	935.48	502.34	934.00	14.00	2471.00	2457.00	25.74
PPT (cm)	169.83	76.81	176.00	24.00	501.00	477.00	3.95
T (C°)	8.33	2.08	8.33	3.33	13.89	10.56	0.11
N deposition (kg^{-1} ha^{-1} yr^{-1}) (Tdep)	3.17	1.26	3.07	1.08	9.32	8.24	0.06
N deposition (kg^{-1} ha^{-1} yr^{-1}) (CMAQ)	3.07	1.23	2.89	1.01	8.48	7.47	0.06
N airscore	4.73	1.68	4.70	1.60	9.60	8.00	0.09
Annual mortality rate (%)*	1.122	0.279	0.002	0.008	0.011	0.003	0.000
Tree DBH	15.03	11.30	10.40	5.00	91.70	86.70	0.58
Tree Height	77.40	46.30	64.00	5.00	260.00	255.00	2.37
Tree LCR	44.30	19.50	40.00	1.00	99.00	98.00	1.00

Note: SCI = Structural complexity index, ΔSCI = change in structural complexity index, SDI = stand density index, SGR = size-growth relationship, CMD = climatic moisture deficit, PPT = mean 10 yr precipitation, T = mean 10 yr temperature, Tdep = National Atmospheric Deposition Program Total deposition estimate, CMAQ = Community Multiscale Air Quality Modeling System.
* Calculated using Sheil and May (1996) formula.

Aspects of our study may have influenced our SGR-stress findings. Our use of periodic growth and space-for-time substitution may obscure important interannual variations within sites (Dye et al., 2019; Klesse et al., 2020). In contrast to most studies on SGR (for an exception, see Dye et al., 2019), our study included largely multi-aged mixed-species stands as well as monocultures. The diversity of regional forests combined with the relative rarity of lichen bioindicator plots did not allow us to investigate composition-driven differences in stress responses. Asynchronous species responses could have buffered stand-level growth against variation in both moisture stress and N deposition (Jucker et al., 2016). Species occurring in our study plots vary considerably in terms of growth sensitivity to N deposition, with *P. ponderosa,* for example, showing a positive carbon increment response, while growth of an otherwise similar species, *P. jeffreyi* Grev. & Balf (Jeffrey pine) is unresponsive (Table A.1; Fenn et al., 2020; Horn et al., 2018). Even within monoculture stands, the climate sensitivity of tree growth varies considerably with tree size and canopy position, and uneven-aged stands typically support more vigorous small-tree growth in canopy gaps as opposed to suppressed trees in even-aged stands (Bowman et al., 2013). The FIA stand age variable does not capture within-stand variation in tree age (Stevens et al., 2016), and the high average values of SCI in our study suggest stands in this study are commonly uneven-aged.

4.3. Linkages between SGR, stand structural complexity, tree growth, and mortality

Size-asymmetric SGR (values > 1) was associated with increasing complexity in stands that were already more structurally complex (i.e., with diameter distributions typical of even-aged stands), suggesting that high SGR reinforced structural complexity. This finding is in agreement with Forrester (2019), who predicted that disproportionately high large-tree growth under high SGR would be expected to increase initial inequalities in tree size as large trees diverge from smaller individuals (Forrester, 2019). In comparison, partial size-symmetric SGR (values < 1) appeared to simplify stand structure in complex stands, consistent with disproportionately rapid small tree growth reducing inequalities in tree size over time. Our analysis of individual-tree volume increment also supported the importance of large tree growth in driving differences in SGR (Pretzsch and Biber, 2010). Growth increased more steeply with initial tree size under high SGR, whereas growth of small trees remained relatively consistent as SGR varied.

We found that structurally simple stands (i.e., with diameter distributions typical of even-aged stands) trended towards increasing complexity under partially size-symmetric SGR, opposite the pattern we observed in complex stands. Rather than high SGR promoting structural complexity by increasing existing inequalities in tree size (Forrester, 2019), Pretzsch and Dieler (2010) predicted that high SGR would diminish structural complexity due to accelerated rates of self-thinning in small trees. Our individual-tree modeling results confirmed that high SGR was associated with self-thinning in smaller trees. Relatively vigorous small-tree growth under low SGR may point to a role of resource-use efficiency in reducing self-thinning or the recruitment of new cohorts as a driver. In a study spanning the same California-Oregon-Washington FIA plot network used in this study, Liang et al. (2007) found that low structural diversity was associated with higher tree recruitment.

We found a strong interaction between SGR and DBH, with high SGR manifesting in terms of rapid large-tree growth. Considered alongside the dramatic decline in large-tree mortality odds under high SGR, our data suggests several possible pathways through which SGR may alter large-tree mortality risk. Disproportionately faster large-tree growth and reduced mortality risk could potentially reflect higher carbohydrate reserves for enduring drought, coupled with greater ability to produce defensive compounds to repel subsequent insect outbreaks (Kolb et al., 2016). However, Bigler and Veblen (2009) found that faster tree growth rates can be associated with lower longevity, which they suggest may reflect poorer tree resistance to pathogens or stem breakage. The susceptibility of fast-growing trees to stem breakage, in particular, would be expected to contribute to tree mortality under N deposition (Fenn et al., 2020). Consequently, competition reduction may be more a plausible explanation than stress resistance for increased large-tree survival under high SGR. A final possibility is that SGR is confounded with structural complexity. Although the relationship was weak, we noted a significant, negative bivariate correlation between SGR and SCI (r^2 = 6%). Low values of SGR would, therefore, be more prevalent in uneven-aged stands, where larger trees are senescent and declining in vigor. Further investigation is needed to isolate the mechanisms through which high SGR may reduce large-tree mortality, as these mechanisms may be important in determining the durability of structural complexity under climate change.

4.4. Direct and indirect drought and N deposition effects on tree growth and mortality

Forrester (2019) proposed a conceptual model in which stress has both direct and mediated effects (via SGR and stand structure) on stand growth. Our individual-tree models provided insights into two elements of stand growth: individual-tree growth and mortality (Liang et al., 2007). We found that N deposition directly impacted individual-tree growth. The limited evidence supporting a unresponsiveness of individual tree mortality to stress in our study was unexpected given that growth, a key predictor of tree mortality risk (Cailleret et al., 2017), was responsive. Nitrogen deposition has been found to have only limited direct effects on individual tree survival (Horn et al., 2018), instead appearing to predispose sensitive species to mortality through increased top kill and stem structural defects (Fenn et al., 2020). Our finding that higher N deposition was associated with higher SGR and, in turn, with greater small-tree mortality suggests that SGR may mediate N deposition effects on tree vigor. One possibility is that higher growth under N deposition creates tree mortality feedbacks through higher stand density. Fertilization typically supports greater stand leaf area index, accelerating rates of stand development and self-thinning mortality (Long et al., 2004). Faster stand densification under N deposition could offset lower mortality odds otherwise associated with improved individual-tree vigor.

We found limited evidence of individual-tree responses to climate and drought, as neither long-term CMD nor shorter-term drought influenced SGR and individual-tree growth. The neutral effect of drought on growth may point to release effects from tree mortality offsetting temporary declines in survivor tree growth. Tree mortality may also have censored trees showing adverse growth impacts of drought from our analysis. Between-site variation in long-term site moisture, as represented by our basic model CMD term, may not be readily distinguishable from forest type or tree species influences, which we included as random effects in modeling. In terms of tree mortality, we found limited evidence for a role of temporarily drier conditions in increasing individual-tree mortality. Our selection of stands free from substantial disturbance, including drought impacts, may have selected for cases where drought impacts were insufficient to reorganize stand growth among survivor trees.

5. Conclusions

Linkages between abiotic stress, SGR and forest structural complexity may be more nuanced than previously hypothesized (Forrester, 2019; Pretzsch and Dieler, 2010), which has implications for the management of western U.S. forests. Stands that were already more structurally complex showed further gains in complexity under high SGR (i.e., disproportionately rapid large-tree growth), whereas stands that were initially simpler structurally increased in complexity under low SGR (i.e., disproportionately slow large tree growth). Thus, the importance of size-dependent tree growth and mortality in fostering structural complexity may differ between simple and complex stands. Because silvicultural prescriptions are often conceived in terms of manipulating tree size distributions (Agee and Skinner, 2005), our findings have implications for the design and durability of silvicultural treatments. Traditional forest fuels treatments typically simplify forest structure by removing small trees that could serve as ladder fuels (Agee and Skinner, 2005). Reductions in ladder fuels may be more durable on high-quality (or moderately N-polluted) sites even if stand density, a major control on canopy bulk density, recovers more quickly. Rapid large tree growth under high site quality may also complement treatments enhancing structural complexity to balance fire risk reduction with objectives such as improving wildlife habitat (Ziegler et al., 2017). Finally, forest managers might consider the historical influence of N deposition on stand development during planning, as well as the likelihood of socioeconomic changes altering N deposition in the future. The positive relationship between SGR and N deposition suggests that, at low-moderate intensities, N pollution impacts on forest stand dynamics are more consistent with fertilization than an abiotic stress effect. Nitrogen inputs from either pollution or fertilization could potentially help maintain wood production in economically and ecologically valuable, large-diameter trees. Experimental studies could establish whether fertilization offers an avenue for intentionally promoting structural complexity and counterbalancing the impacts of stressors, such as drought and insects and diseases, in these systems.

CRediT authorship contribution statement

Christopher E. Looney: Conceptualization, Methodology, Formal analysis, Visualization, Writing - original draft. **Anthony W. D'Amato:** Conceptualization, Methodology, Writing - original draft. **Sarah Jovan:** Conceptualization, Methodology, Data curation, Resources, Writing - original draft.

Declaration of Competing Interest

The authors declare that they have no known competing financial interests or personal relationships that could have appeared to influence the work reported in this paper.

Acknowledgements

Support for this research was provided by the USDA Forest Service Pacific Southwest Research Station, the University of Vermont Rubenstein School of Environment and Natural Resources, and the USDA Forest Service Pacific Northwest Research Station. Andrew Gray and Wilfred Previant provided advice on the FIA database, Mark Fenn and Margaret Evans on air pollution and climate, and Nels Johnson on statistical modeling. The rFIA package for R developed by Hunter Stanke facilitated the estimation of forest variables from the FIA dataset. Thanks to the participants in the 2020 Western Mensurationists Conference whose comments on a previous version greatly improved the manuscript. Aspects of the study design grew out of research on Colorado forests conducted with Linda Nagel and the Adaptive Silviculture for Climate Change Network.

Appendix

See Figs. A.1 and A.2, Tables A.1–A.3.

References

Abatzoglou, J.T., Dobrowski, S.Z., Parks, S.A., Hegewisch, K.C., 2018. TerraClimate, a high-resolution global dataset of monthly climate and climatic water balance from 1958–2015. Sci. Data 5, 170191. https://doi.org/10.1038/sdata.2017.191.

Agee, J.K., Skinner, C.N., 2005. Basic principles of forest fuel reduction treatments Relative Risk Assessments for Decision –Making Related To Uncharacteristic Wildfire. For. Ecol. Manag. 211, 83–96. https://doi.org/10.1016/j.foreco.2005.01.034.

Aitchison, J., 1986. The Statistical Analysis of Compositional Data. Springer, Netherlands, Dordrecht.

Baret, M., Pepin, S., Ward, C., Pothier, D., 2017. Long-term changes in stand growth dominance as related to resource acquisition and utilization in the boreal forest. For. Ecol. Manag. 400, 408–416. https://doi.org/10.1016/j.foreco.2017.06.026.

Bartoń, K., 2017. MuMln: Multi-model inference. R Package Version 1 (40).

Bauhus, J., Puettmann, K., Messier, C., 2009. Silviculture for old-growth attributes, Old forests, new management: the conservation and use of old-growth forests in the 21st century. For. Ecol. Manag. 258, 525–537. https://doi.org/10.1016/j.foreco.2009.01.053.

Bechtold, W.A., Patterson, P.L. (Eds.), 2005. The enhanced forest inventory and analysis program - national sampling design and estimation procedures. Gen Tech Rep SRS-80 US Dep. Agric. For. Serv. South. Res. Stn. Ashville NC. https://doi.org/10.2737/SRS-GTR-80.

Bigler, C., Veblen, T.T., 2009. Increased early growth rates decrease longevities of conifers in subalpine forests. Oikos 118, 1130–1138. https://doi.org/10.1111/j.1600-0706.2009.17592.x.

Binkley, D., 2004. A hypothesis about the interaction of tree dominance and stand production through stand development. For. Ecol. Manag. 190, 265–271. https://doi.org/10.1016/j.foreco.2003.10.018.
Binkley, D., Kashian, D.M., Boyden, S., Kaye, M.W., Bradford, J.B., Arthur, M.A., Fornwalt, P.J., Ryan, M.G., 2006. Patterns of growth dominance in forests of the Rocky Mountains. USA. For. Ecol. Manag. 236, 193–201. https://doi.org/10.1016/j.foreco.2006.09.001.
Bobbink, R., Hicks, K., Galloway, J., Spranger, T., Alkemade, R., Ashmore, M., Bustamante, M., Cinderby, S., Davidson, E., Dentener, F., Emmett, B., Erisman, J.-W., Fenn, M., Gilliam, F., Nordin, A., Pardo, L., Vries, W.D., 2010. Global assessment of nitrogen deposition effects on terrestrial plant diversity: a synthesis. Ecol. Appl. 20, 30–59. https://doi.org/10.1890/08-1140.1.
Bottero, A., D'Amato, A.W., Palik, B.J., Bradford, J.B., Fraver, S., Battaglia, M.A., Asherin, L.A., 2017. Density-dependent vulnerability of forest ecosystems to drought. J. Appl. Ecol. 54, 1605–1614. https://doi.org/10.1111/1365-2664.12847.
Bowman, D.M.J.S., Brienen, R.J.W., Gloor, E., Phillips, O.L., Prior, L.D., 2013. Detecting trends in tree growth: not so simple. Trends Plant Sci. 18, 11–17. https://doi.org/10.1016/j.tplants.2012.08.005.
Bowman, W.D., Cleveland, C.C., Halada, Ľ., Hreško, J., Baron, J.S., 2008. Negative impact of nitrogen deposition on soil buffering capacity. Nat. Geosci. 1, 767–770. https://doi.org/10.1038/ngeo339.
Bradford, J.B., D'Amato, A.W., Palik, B.J., Fraver, S., 2010. A new method for evaluating forest thinning: growth dominance in managed Pinus resinosa stands. Can. J. For. Res. 40, 843–849. https://doi.org/10.1139/X10-039.
Burnham, K.P., Anderson, D.R., 2002. Model Selection and Multimodel Inference: A Practical Information-Theoretic Approach, 2nd ed. Springer-Verlag, New York.
Cailleret, M., Jansen, S., Robert, E.M.R., Desoto, L., Aakala, T., Antos, J.A., Beikircher, B., Bigler, C., Bugmann, H., Caccianiga, M., Čada, V., Camarero, J.J., Cherubini, P., Cochard, H., Coyea, M.R., Čufar, K., Das, A.J., Davi, H., Delzon, S., Dorman, M., Gea-Izquierdo, G., Gillner, S., Haavik, L.J., Hartmann, H., Hereş, A.-M., Hultine, K.R., Janda, P., Kane, J.M., Kharuk, V.I., Kitzberger, T., Klein, T., Kramer, K., Lens, F., Levanic, T., Linares Calderon, J.C., Lloret, F., Lobo-Do-Vale, R., Lombardi, F., López Rodríguez, R., Mäkinen, H., Mayr, S., Mészáros, I., Metsaranta, J.M., Minunno, F., Oberhuber, W., Papadopoulos, A., Peltoniemi, M., Petritan, A.M., Rohner, B., Sangüesa-Barreda, G., Sarris, D., Smith, J.M., Stan, A.B., Sterck, F., Stojanović, D.B., Suarez, M.L., Svoboda, M., Tognetti, R., Torres-Ruiz, J.M., Trotsiuk, V., Villalba, R., Vodde, F., Westwood, A.R., Wyckoff, P.H., Zafirov, N., Martínez-Vilalta, J., 2017. A synthesis of radial growth patterns preceding tree mortality. Glob. Change Biol. 23, 1675–1690. https://doi.org/10.1111/gcb.13535.
Carter, T.S., Clark, C.M., Fenn, M.E., Jovan, S., Perakis, S.S., Riddell, J., Schaberg, P.G., Greaver, T.L., Hastings, M.G., 2017. Mechanisms of nitrogen deposition effects on temperate forest lichens and trees. Ecosphere 8, e01717. https://doi.org/10.1002/ecs2.1717.
Castagneri, D., Nola, P., Cherubini, P., Motta, R., 2012. Temporal variability of size–growth relationships in a Norway spruce forest: the influences of stand structure, logging, and climate. Can. J. For. Res. 42, 550–560. https://doi.org/10.1139/x2012-007.
Clark, C.M., Bell, M.D., Boyd, J.W., Compton, J.E., Davidson, E.A., Davis, C., Fenn, M.E., Geiser, L., Jones, L., Blett, T.F., 2017. Nitrogen-induced terrestrial eutrophication: cascading effects and impacts on ecosystem services. Ecosphere 8, e01877. https://doi.org/10.1002/ecs2.1877.
Crookston, N.L., Dixon, G.E., 2005. The forest vegetation simulator: A review of its structure, content, and applications. Comput. Electron. Agric. Decision Support Syst. For. Manage. 49, 60–80. https://doi.org/10.1016/j.compag.2005.02.003.
Dănescu, A., Albrecht, A.T., Bauhus, J., Kohnle, U., 2017. Geocentric alternatives to site index for modeling tree increment in uneven-aged mixed stands. For. Ecol. Manag. 392, 1–12. https://doi.org/10.1016/j.foreco.2017.02.045.
del Río, M., Condés, S., Pretzsch, H., 2014. Analyzing size-symmetric vs. size-asymmetric and intra- vs. inter-specific competition in beech (Fagus sylvatica L.) mixed stands. For. Ecol. Manag. 325, 90–98. https://doi.org/10.1016/j.foreco.2014.03.047.
Doi, B.T., Binkley, D., Stape, J.L., 2010. Does reverse growth dominance develop in old plantations of *Eucalyptus saligna*? For. Ecol. Manage. Product. Tropical Plantations 259, 1815–1818. https://doi.org/10.1016/j.foreco.2009.05.031.
Ducey, M.J., 2009. The ratio of additive and traditional stand density indices. West. J. Appl. For. 24, 5–10. https://doi.org/10.1093/wjaf/24.1.5.
Dye, A., Ross Alexander, M., Bishop, D., Druckenbrod, D., Pederson, N., Hessl, A., 2019. Size–growth asymmetry is not consistently related to productivity across an eastern US temperate forest network. Oecologia 189, 515–528. https://doi.org/10.1007/s00442-018-4318-9.
Ellison, G.N., Gotelli, N.J., 2004. A Primer of Ecological Statistics. Sinauer Sunderland Mass, USA.
Fenn, M.E., Preisler, H.K., Fried, J.S., Bytnerowicz, A., Schilling, S.L., Jovan, S., Kuegler, O., 2020. Evaluating the effects of nitrogen and sulfur deposition and ozone on tree growth and mortality in California using a spatially comprehensive forest inventory. For. Ecol. Manag. 465, 118084 https://doi.org/10.1016/j.foreco.2020.118084.
Forrester, D.I., 2019. Linking forest growth with stand structure: Tree size inequality, tree growth or resource partitioning and the asymmetry of competition. For. Ecol. Manag. 447, 139–157. https://doi.org/10.1016/j.foreco.2019.05.053.
Franklin, J.F., Mitchell, R.J., Palik, B.J., et al., 2007. Natural disturbance and stand development principles for ecological forestry. Gen Tech Rep NRS-19 US Dep Agric. For. Serv. North. Res. Stn. Newton Sq. PA. https://doi.org/10.2737/NRS-GTR-19.
Geiser, L.H., Nelson, P.R., Jovan, S.E., Root, H.T., Clark, C.M., 2019. Assessing ecological risks from atmospheric deposition of nitrogen and sulfur to US forests using epiphytic macrolichens. Divers. 116 (87–11), 87. https://doi.org/10.3390/d11060087.
Gower, S.T., McMurtrie, R.E., Murty, D., 1996. Aboveground net primary production decline with stand age: potential causes. Trends Ecol. Evol. 11, 378–382. https://doi.org/10.1016/0169-5347(96)10042-2.
Hartig, F., 2018. DHARMa: residual diagnostics for hierarchical (multi-level/mixed) regression models: R package version 0.20.
Hijmans, R.J., Etten, J. van, Sumner, M., Cheng, J., Baston, D., Bevan, A., Bivand, R., Busetto, L., Canty, M., Fasoli, B., Forrest, D., Ghosh, A., Golicher, D., Gray, J., Greenberg, J.A., Hiemstra, P., Hingee, K., Geosciences, I. for M.A., Karney, C., Mattiuzzi, M., Mosher, S., Nowosad, J., Pebesma, E., Lamigueiro, O.P., Racine, E.B., Rowlingson, B., Shortridge, A., Venables, B., Wueest, R., 2020. raster: Geographic Data Analysis and Modeling. R package version 3.4-5.
Horn, K.J., Thomas, R.Q., Clark, C.M., Pardo, L.H., Fenn, M.E., Lawrence, G.B., Perakis, S.S., Smithwick, E.A.H., Baldwin, D., Braun, S., Nordin, A., Perry, C.H., Phelan, J.N., Schaberg, P.G., Clair, S.B.S., Warby, R., Watmough, S., 2018. Growth and survival relationships of 71 tree species with nitrogen and sulfur deposition across the conterminous U.S. PLOS ONE 13, e0205296. https://doi.org/10.1371/journal.pone.0205296.
Ibáñez, I., Zak, D.R., Burton, A.J., Pregitzer, K.S., 2018. Anthropogenic nitrogen deposition ameliorates the decline in tree growth caused by a drier climate. Ecology 99, 411–420. https://doi.org/10.1002/ecy.2095.
James, G., Witten, D., Hastie, T., Tibshirani, R., 2013. An Introduction to Statistical Learning: with Applications in R, Springer Texts in Statistics. Springer-Verlag, New York, 10.1007/978-1-4614-7138-7.
Jovan, S., 2008. Lichen bioindication of biodiversity, air quality, and climate: baseline results from monitoring in Washington, Oregon, and California. Gen Tech Rep PNW-GTR-737 Portland US Dep. Agric. For. Serv. Pac. Northwest Res. Stn. 115 P 737, 83. https://doi.org/10.2737/PNW-GTR-737.
Jovan, S., Fenn, M.E., Buhler, M., Bytnerowicz, A., Kovasi, A., Hutten, M., DiMeglio, E., Schweizer, D., 2021. Challenges characterizing N deposition to high elevation protected areas: A case study integrating instrument, simulated, and lichen inventory datasets for the Devils Postpile National Monument and surrounding region, USA. Ecol. Indic. 122, 107311 https://doi.org/10.1016/j.ecolind.2020.107311.
Jovan, S., Geiser, L.H., Dillman, K., Halderman, M., Shory, R., 2020. User guide for the national Forest Inventory and Analysis lichen database (ver. 1.0)., Gen. Tech. Rep. U. S. Department of Agriculture, Forest Service, Pacific Northwest Research Station, Portland, OR.
Jucker, T., Avăcăriţei, D., Bărnoaiea, I., Duduman, G., Bouriaud, O., Coomes, D.A., 2016. Climate modulates the effects of tree diversity on forest productivity. J. Ecol. 104, 388–398. https://doi.org/10.1111/1365-2745.12522.
Klesse, S., DeRose, R.J., Babst, F., Black, B.A., Anderegg, L.D.L., Axelson, J., Ettinger, A., Griesbauer, H., Guiterman, C.H., Harley, G., Harvey, J.E., Lo, Y.-H., Lynch, A.M., O'Connor, C., Restaino, C., Sauchyn, D., Shaw, J.D., Smith, D.J., Wood, L., Villanueva-Díaz, J., Evans, M.E.K., 2020. Continental-scale tree-ring-based projection of Douglas-fir growth: Testing the limits of space-for-time substitution. Glob. Change Biol. 26 https://doi.org/10.1111/gcb.15170.
Kolb, T.E., Fettig, C.J., Ayres, M.P., Bentz, B.J., Hicke, J.A., Mathiasen, R., Stewart, J.E., Weed, A.S., 2016. Observed and anticipated impacts of drought on forest insects and diseases in the United States. For. Ecol. Manag Special Sec.: Drought US For.: Impacts Potential Manage. Responses 380, 321–334. https://doi.org/10.1016/j.foreco.2016.04.051.
Li, W., Hartmann, H., Adams, H.D., Zhang, H., Jin, C., Zhao, C., Guan, D., Wang, A., Yuan, F., Wu, J., 2018. The sweet side of global change–dynamic responses of non-structural carbohydrates to drought, elevated CO2 and nitrogen fertilization in tree species. Tree Physiol. 38, 1706–1723. https://doi.org/10.1093/treephys/tpy059.
Liang, J., Buongiorno, J., Monserud, R.A., Kruger, E.L., Zhou, M., 2007. Effects of diversity of tree species and size on forest basal area growth, recruitment, and mortality. For. Ecol. Manag. 243, 116–127. https://doi.org/10.1016/j.foreco.2007.02.028.
Long, J.N., Daniel, T.W., 1990. Assessment of growing stock in uneven-aged stands. West. J. Appl. For. 5, 93–96. https://doi.org/10.1093/wjaf/5.3.93.
Long, J.N., Dean, T.J., Roberts, S.D., 2004. Linkages between silviculture and ecology: examination of several important conceptual models. For. Ecol. Manag. 200, 249–261. https://doi.org/10.1016/j.foreco.2004.07.005.
Looney, C.E., D'Amato, A.W., Fraver, S., Palik, B.J., Reinikainen, M.R., 2016. Examining the influences of tree-to-tree competition and climate on size-growth relationships in hydric, multi-aged Fraxinus nigra stands. For. Ecol. Manag. 375, 238–248. https://doi.org/10.1016/j.foreco.2016.05.050.
Lutz, J.A., van Wagtendonk, J.W., Franklin, J.F., 2010. Climatic water deficit, tree species ranges, and climate change in Yosemite National Park. J. Biogeogr. 37, 936–950. https://doi.org/10.1111/j.1365-2699.2009.02268.x.
Magnusson, A., Skaug, H., Berg, C., Kristensen, M., van Bentham, K., Bolker, B., Brooks, M., 2018. glmmTMB: generalized linear mixed models using Template Model Builder. R package version 0.2.2.0.
McCune, B., 2007. Improved estimates of incident radiation and heat load using non-parametric regression against topographic variables. J. Veg. Sci. 18, 751–754. https://doi.org/10.1111/j.1654-1103.2007.tb02590.x.
Metsaranta, J.M., 2020. Influence of past mortality and measurement thresholds on tree-ring inferred trends in tree distribution and size-growth relationships at a Populus tremuloides stand in the Northwest Territories. Canada. For. Ecol. Manag. 466, 118138 https://doi.org/10.1016/j.foreco.2020.118138.
Metsaranta, J.M., Lieffers, V.J., 2010. Patterns of inter-annual variation in the size asymmetry of growth in Pinus banksiana. Oecologia 163, 737–745. https://doi.org/10.1007/s00442-009-1559-7.
Muller, J.J., Nagel, L.M., Palik, B.J., 2019. Forest adaptation strategies aimed at climate change: Assessing the performance of future climate-adapted tree species in a

northern Minnesota pine ecosystem. For. Ecol. Manag. 451, 117539 https://doi.org/10.1016/j.foreco.2019.117539.
Nagel, L.M., Palik, B.J., Battaglia, M.A., D'Amato, A.W., Guldin, J.M., Swanston, C.W., Janowiak, M.K., Powers, M.P., Joyce, L.A., Millar, C.I., Peterson, D.L., Ganio, L.M., Kirschbaum, C., Roske, M.R., 2017. Adaptive Silviculture for Climate Change: A national experiment in manager-scientist partnerships to apply an adaptation framework. J. For. 115, 167–178. https://doi.org/10.5849/jof.16-039.
Palmer, W.C., 1965. Meteorological drought. U.S. Weather Bureau Office of Climatology, Washington, D.C.
Pothier, D., 2017. Relationships between patterns of stand growth dominance and tree competition mode for species of various shade tolerances. For. Ecol. Manag. 406, 155–162. https://doi.org/10.1016/j.foreco.2017.09.066.
Preisler, H.K., Grulke, N.E., Heath, Z., Smith, S.L., 2017. Analysis and out-year forecast of beetle, borer, and drought-induced tree mortality in California. For. Ecol. Manag. 399, 166–178. https://doi.org/10.1016/j.foreco.2017.05.039.
Pretzsch, H., Biber, P., 2010. Size-symmetric versus size-asymmetric competition and growth partitioning among trees in forest stands along an ecological gradient in central Europe. Can. J. For. Res. 40, 370–384. https://doi.org/10.1139/X09-195.
Pretzsch, H., Dieler, J., 2010. The dependency of the size-growth relationship of Norway spruce (Picea abies [L.] Karst.) and European beech (Fagus sylvatica [L.]) in forest stands on long-term site conditions, drought events, and ozone stress. Trees 25, 355–369. https://doi.org/10.1007/s00468-010-0510-1.
PRISM Climate Group, 2019. PRISM climate data [WWW Document]. Northwest Alliance Comput. Sci. Eng. URL http://www.prism.oregonstate.edu/recent/ (accessed 8.11.19).
Puettmann, K.J., D'Amato, A.W., Kohnle, U., Bauhus, J., 2009. Individual-tree growth dynamics of mature Abies alba during repeated irregular group shelterwood (Femelschlag) cuttings. Can. J. For. Res. 39, 2437–2449. https://doi.org/10.1139/X09-158.
R Core Team, 2018. R: A language and environment for statistical computing. R Foundation for Statistical Computing, Vienna, Austria.
Raymond, P., Bédard, S., Roy, V., Larouche, C., Tremblay, S., 2009. The irregular system: Review, classification, and potential application to forests affected by partial disturbances. J. For. 107, 405–413.
Reineke, L.H., 1933. Perfecting a stand-density index for even-aged forests. J. Agric. Res. 46, 627–638.
Restaino, C.M., Peterson, D.L., Littell, J., 2016. Increased water deficit decreases Douglas fir growth throughout western US forests. Proc. Natl. Acad. Sci. 113, 9557–9562. https://doi.org/10.1073/pnas.1602384113.
Richards, S.A., 2008. Dealing with overdispersed count data in applied ecology. J. Appl. Ecol. 45, 218–227. https://doi.org/10.1111/j.1365-2664.2007.01377.x.
Root, H.T., Geiser, L.H., Jovan, S., Neitlich, P., 2015. Epiphytic macrolichen indication of air quality and climate in interior forested mountains of the Pacific Northwest. USA. Ecol. Indic. 53, 95–105. https://doi.org/10.1016/j.ecolind.2015.01.029.
Sheil, D., May, R.M., 1996. Mortality and recruitment rate evaluations in heterogeneous tropical forests. J. Ecol. 84, 91–100. https://doi.org/10.2307/2261703.
Smith, F.W., Long, J.N., 2001. Age-related decline in forest growth: an emergent property. For. Ecol. Manag. 144, 175–181. https://doi.org/10.1016/S0378-1127(00)00369-8.
Stephenson, N., 1998. Actual evapotranspiration and deficit: biologically meaningful correlates of vegetation distribution across spatial scales. J. Biogeogr. 25, 855–870. https://doi.org/10.1046/j.1365-2699.1998.00233.x.
Stevens, J.T., Safford, H.D., North, M.P., Fried, J.S., Gray, A.N., Brown, P.M., Dolanc, C. R., Dobrowski, S.Z., Falk, D.A., Farris, C.A., Franklin, J.F., Fulé, P.Z., Hagmann, R.K., Knapp, E.E., Miller, J.D., Smith, D.F., Swetnam, T.W., Taylor, A.H., 2016. Average stand age from forest inventory plots does not describe historical fire regimes in ponderosa pine and mixed-conifer forests of western North America. PLOS ONE 11, e0147688. https://doi.org/10.1371/journal.pone.0147688.
Sugiura, N., 1978. Further analysts of the data by Akaike's information criterion and the finite corrections. Commun. Stat. - Theory Methods 7, 13–26. https://doi.org/10.1080/03610927808827599.
Trouillier, M., van der Maaten-Theunissen, M., Scharnweber, T., Würth, D., Burger, A., Schnittler, M., Wilmking, M., 2019. Size matters—a comparison of three methods to assess age- and size-dependent climate sensitivity of trees. Trees 33, 183–192. https://doi.org/10.1007/s00468-018-1767-z.
van Kuijk, M., Anten, N.P.R., Oomen, R.J., van Bentum, D.W., Werger, M.J.A., 2008. The limited importance of size-asymmetric light competition and growth of pioneer species in early secondary forest succession in Vietnam. Oecologia 157, 1–12. https://doi.org/10.1007/s00442-008-1048-4.
Waddel, K., 2013. PNW-FIADB Users Manual: A data dictionary and user guide for the PNW-FIADB database. Pacific Northwest Research Station, Portland, OR.
Walker, J.T., Beachley, G., Amos, H.M., Baron, J.S., Bash, J., Baumgardner, R., Bell, M. D., Benedict, K.B., Chen, X., Clow, D.W., Cole, A., Coughlin, J.G., Cruz, K., Daly, R. W., Decina, S.M., Elliott, E.M., Fenn, M.E., Ganzeveld, L., Gebhart, K., Isil, S.S., Kerschner, B.M., Larson, R.S., Lavery, T., Lear, G.G., Macy, T., Mast, M.A., Mishoe, K., Morris, K.H., Padgett, P.E., Pouyat, R.V., Puchalski, M., Pye, H.O.T., Rea, A.W., Rhodes, M.F., Rogers, C.M., Saylor, R., Scheffe, R., Schichtel, B.A., Schwede, D.B., Sexstone, G.A., Sive, B.C., Sosa Echeverría, R., Templer, P.H., Thompson, T., Tong, D., Wetherbee, G.A., Whitlow, T.H., Wu, Z., Yu, Z., Zhang, L., 2019. Toward the improvement of total nitrogen deposition budgets in the United States. Sci. Total Environ. 691, 1328–1352. https://doi.org/10.1016/j.scitotenv.2019.07.058.
Wang, T., Hamann, A., Spittlehouse, D., Carroll, C., 2016. Locally downscaled and spatially customizable climate data for historical and future periods for North America. PLOS ONE 11, e0156720. https://doi.org/10.1371/journal.pone.0156720.
Western Regional Climate Center, 2021. Narratives by State [WWW Document]. URL https://wrcc.dri.edu (accessed 4.19.21).
Woudenberg, S.W., Conkling, B.L., O'Connell, B.M., LaPoint, E.B., Turner, J.A., Waddell, K.L., 2010. The Forest Inventory and Analysis Database: Database description and users manual version 4.0 for Phase 2. U.S. Department of Agriculture, Forest Service, Rocky Mountain Research Station, Fort Collins, CO.
Zarnoch, S.J., Bechtold, W.A., Stolte, K.W., 2004. Using crown condition variables as indicators of forest health. Can. J. For. Res. 34, 1057–1070. https://doi.org/10.1139/x03-277.
Zhang, J., Finley, K.A., Johnson, N.G., Ritchie, M.W., 2019. Lowering Stand Density Enhances Resiliency of Ponderosa Pine Forests to Disturbances and Climate Change. For. Sci. 65, 496–507. https://doi.org/10.1093/forsci/fxz006.
Zhang, J., Ritchie, M.W., Maguire, D.A., Oliver, W.W., 2013. Thinning ponderosa pine (Pinus ponderosa) stands reduces mortality while maintaining stand productivity. Can. J. For. Res. 43, 311–320. https://doi.org/10.1139/cjfr-2012-0411.
Ziegler, J.P., Hoffman, C., Battaglia, M., Mell, W., 2017. Spatially explicit measurements of forest structure and fire behavior following restoration treatments in dry forests. For. Ecol. Manag. 386, 1–12. https://doi.org/10.1016/j.foreco.2016.12.002.